Fluid-structure interaction study of bio-magnetic fluid in a wavy bifurcated channel with elastic walls

Hasan Shahzad[1]*, Xinhua Wang[1]*, Zehba Raizah[2,3],
Arshad Riaz[4], Afraz Hussain Majeed[5],
Muhammad Adnan Anwar[6] and Sayed M. Eldin [7]

[1]Faculty of Materials and Manufacturing, College of Mechanical Engineering and Applied Electronics Technology, Beijing University of Technology, Beijing, China, [2]Department of Mathematics, College of Science, King Khalid University, Abha, Saudi Arabia, [3]Research Center for Advanced Materials Science (RCAMS), King Khalid University, Abha, Saudi Arabia, [4]Division of Science and Technology, Department of Mathematics, University of Education, Lahore, Pakistan, [5]Department of Mathematics, Air University, Islamabad, Pakistan, [6]Department of Mathematics, Syed Babar Ali School of Science and Engineering, Lahore, Pakistan, [7]Center of Research, Faculty of Engineering, Future University in Egypt, New Cairo, Egypt

As a result of its wide range of applications, FSI has grabbed the attention of researchers and scientists. In this study we consider an incompressible, laminar fluid flowing through the bifurcated channel. The wavy walls of the channel are considered elastic. Moreover, a magnetic field is applied towards the axial direction of the flow. Using a two-way fluid-structure interaction, an Arbitrary Lagrangian-Eulerian (ALE) formulation is used for coupling the problem. The problem is discretized using P_2 and P_1 finite element methods to approximate the displacement, pressure, and velocity. The linearized system of equations is solved using Newton's iterative scheme. The analysis is carried out for the Reynolds number and Hartman number. The ranges of the studied parameters are Reynolds number $300 \leq Re \leq 1000$ and Hartmann number $0 \leq Ha \leq 10$. The hemodynamic effects on the bifurcated channel and elastic walls are calculated using velocity, pressure, wall shear stresses (WSS), and loads at the walls. The study shows there is an increase in boundary load as the values of the Hartman number increase hence WSS increases. On the other hand, an increase in the Reynolds number increases the resistance forces hence velocity and WSS decrease. Also, numerical values of WSS for rigid and elastic walls are calculated. Studies showed that WSS decreases for the FSI case when compare to CFD (computational fluid dynamic) case.

KEYWORDS

fluid-structure interaction, wall shear stress, finite element method, bifurcation, biomagnetic fluid, elastic walls

Introduction

Cardiovascular disorders are now the leading cause of death worldwide, accounting for around a quarter of all deaths in the modern era [1–3]. Cardiovascular problems include atherosclerosis, carotid aneurysm, and deep vein thrombosis, which cause heart attack, stroke, and embolism all stem from platelet aggregation [4]. Recent years have seen a large number of theoretical and experimental studies on arterial blood flow [4]. To better understand how the cardiovascular system's physiological blood flow might be diagnosed, researchers are eager to examine how blood flows through an aortic artery bifurcation. The evaluation of blood flow through different types of geometries under different flow sites is highly essential because the leading cause of death in the world by arterial diseases is connected with the flow problems in the blood arteries. Viscosity, size, and form of arteries, as well as flow characteristics such as laminar, pulsatile, and turbulent all, have a significant impact on how blood moves through the vessels [5]. Numerous theoretical and experimental investigations on arterial blood flow have been conducted recently. Blood flow hemodynamics strongly depends upon the non-Newtonian characteristics, flow behavior, and shape of the artery. Fojas et al.[6] study the two-dimensional carotid artery model with bifurcation. An arbitrary Lagrangian-Eulerian (ALE) technique was used to solve the system of nonlinear equations. Comparisons were made between the findings of the hemodynamic simulations and the Doppler ultrasonography measurements of physiological blood velocity.

A literature review shows that many experiments were performed to measure the velocity field in bifurcation [7, 8], and the pressure drop model was proposed [9, 10]. Mekheimer [11] Proposed a theoretical investigation of a mixture of blood and synovial with heat distribution, volume fraction and concentration effects through stenosed concentric tubes. They concluded synovial fluid which has less friction than other fluids, can help to speed up the blood flow in the area of atherosclerosis. Flow past in a branching tube was analyzed by [12]. Yung et al. [13] numerically investigated the flow in bifurcation. For analytical and numerical research, basic "Y" type bifurcations with sharp corners were taken as assumptions, but experimental articles did not specify specific geometry employed in experiments. Thus, it is only possible to study the correlation between these theoretical and experimental results qualitatively. For the first time [14, 15], conducted thorough experiments to explore the primary and secondary flow field in a single bifurcation with smoothed corners and precisely defined geometric parameters. Numerical simulation performed by Zhao et al. [16] showed agreement between experimental and computational results by [14, 15].

Magnetohydrodynamics (MHD) is the study of fluids with magnetic characteristics. Human blood flow in the vascular system is greatly influenced by the use of MHD. Magnetic devices have been developed for a variety of applications, including medication transporters, cancer treatment, cell separation, etc. In medical research, the theory of electromagnetic field was first introduced by Kolin [17]. Later, Korchevskii, Marochnik [18] offered the opportunity to control the blood flow in the arterial lumen system by spreading a magnetic field. Ahmed et al. [19] proposed a unique model of unsteady MHD fluid flow and heat transfer across carbon nanotubes utilizing variable viscosity. MHD effects on blood flow in bifurcated arteries with minor stenosis in the parent lumen were studied by Srinivasacharya and Rao [20]. They used the finite difference method to solve the resulting set of equations numerically. The hemodynamics effects like flow rate, shear stresses are calculated for the involved parameter. Abdelsalam et al.[21] investigated the effects of chemical interaction and laser radiation with MHD and electroosmotic flow of non-Newtonian hybrid fluid in a sinusoidal channel. The aim of the research is to help restrict the growth of bacteria, promote oxygen binding to the blood, transfer oxygen to organs, and activate white blood cells. Mekheimer et al. [11] used a vertical micro channel to investigate the effect of diamond and copper nanoparticles on the electro-magneto-hydro dynamically regulated peristaltic pumping of a couple stress fluid. They found the irreversibility process enhanced with the sphere shaped particles also, MHD reduced the bolus size. Further investigation on MHD flows and their applications can be seen in the articles [22–25] and references therein.

Researchers are eager to examine how blood flows through an aortic artery bifurcation to better understand how the cardiovascular system's physiological blood flow might be diagnosed. Blood flow across diverse geometries and flow sites are critical since arterial diseases are the leading cause of death in the globe, and because flow problems in the blood arteries are the primary cause of death. The blood flow is greatly affected by physical properties such as viscosity, vessel size and shape, and flow behaviour, such as laminar or pulsatile. Many vascular disorders can be linked back to abnormal blood flow dynamics in the arteries. Having a better knowledge of these dynamics could help in both healthy and pathological conditions. The hemodynamics of blood flow cannot be predicted accurately if we assume rigid walls. So this study is not effective in many practical cases. Therefore, FSI is taken into account [26]. FSI between blood and wall artery is difficult to model. Both modeling and computing efficiency is advancing rapidly in this discipline. Taking into consideration the FSI for the vessels and blood can be achieved by introducing a 2D or 3D elastic structure, utilizing a Lagrangian [27], Eulerian [28], or ALE (Arbitrary Lagrangian-Eulerian) framework [29]. Zhao et al. [30] studied the blood flow in the aortic arch using FSI. The system of equations is formed using the ALE frame. They studied the elasticity and wall stress in the aorta wall. Studies show that difference in the elastic characteristics of the different layer is responsible for the pathological state. Methods et al. [31]
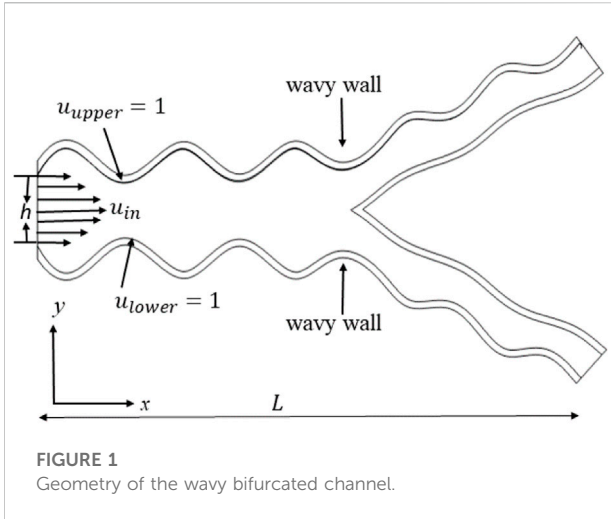
FIGURE 1
Geometry of the wavy bifurcated channel.

FIGURE 2
Coarse mesh for the discused problem.

performed an FSI simulation in a patient-specific artery using the ALE concept. The fluid flow pattern and WSS were given special consideration in their study. In [32] the hemodynamics characteristic of blood flow using FSI were discussed. The coupling of the non-linear system of the equation with FSI is performed using the Gauss-Seidel iterative algorithm. Recently Shahzad et al. [33] studied the hemodynamics effects of non-Newtonian fluid flowing in the bifurcated artery. The theoretical model for stenosed bifurcated artery was constructed. They used an ALE technique to study the elastic wall behavior for non-Newtonian fluid.

In this study, a fluid-structure interaction simulation is performed for the bifurcated channel. The walls of the channel are considered wavy and elastic. The magnetic field is applied toward the axial direction of the flow. How Re and Ha affect the hemodynamics of the channel were studied. In the next section, physical configuration and mathematical modeling are performed. After that solution methodology is explained. The result and discussion section highlighted the major outcomes of the study. The conclusion based on the results is highlighted in the last section.

Physical configuration and mathematical modeling

The coordinate system and the geometry of the problem are shown in Figure 1. The wall of the channel is considered wavy with width $w = 0.08 cm$. The total length of the channel is $L = 6 cm$. The geometrical elements that influence the fluid dynamics in branching geometries are: change in cross-sectional area from mother to daughter branch, shape change in bifurcation module, flow driven at a bifurcation, and flow path curvature in the bifurcation module. Further, we suppose that walls of the bifurcated channel are constructed of linear elastic
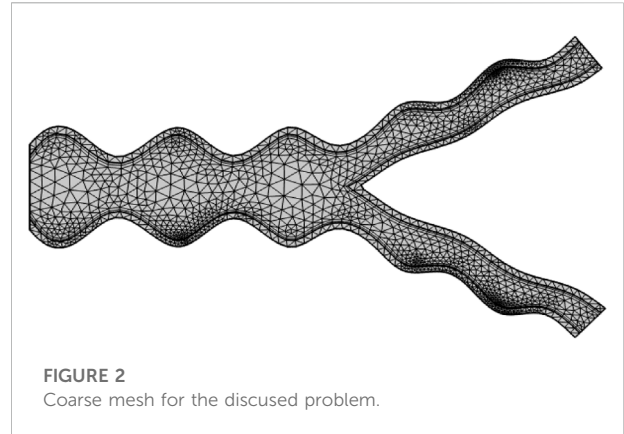
and isotropic material with a particular Young's modulus and Poisson ratio. Which we defined as [34]

$$v = \frac{\lambda_l}{2(\lambda + \mu_m)}, \quad E = \frac{\mu(3\lambda_l + 2\mu_m)}{\lambda_l + \mu_m},$$
$$\mu_m = \frac{E}{2(1 + v)}, \quad \lambda_l = \frac{vE}{(1 + \mu_m)(1 - 2v)} \quad (1)$$

where λ_l, Lame coefficient; μ_m, Shear modulus; E, Young's Modulus; v, Poisson ratio. Where $E = 5 \times 10^5$ and value of $v = 0.49$.

We consider the incompressible, two–dimensional, viscous, biomagnetic fluid flowing through the bifurcated channel. The walls of the bifurcated channel are considered wavy. The upper wall and lower walls move with velocity 1. The parabolic inlet with $U_{max} = 0.3$ is considered at the inlet. While at outlet boundaries pressure is assumed zero. The low magnetic Reynolds approximation is assumed [35].

Lagrangian and Eulerian descriptions are commonly used in continuum mechanics to describe solid and fluid motion, respectively. With regards to fluid and solid domains mixing (fluid structure interaction), ALE is a more generic approach. For the fluid-structure interaction, we can write the governing equations in two dimensions as [34].

TABLE 1 Grid convergence for various refinement levels at Re = 200 and Ha = 0.

Refinement level	WSS on the upper wall	Absolute error
1	0.473018	—
2	0.470492	0.0025
3	0.473178	0.0027
4	0.475150	0.0047
5	0.476230	0.0011
6	0.476365	0.0001

TABLE 2 WSS comparison for CFD and FSI case.

| Ha	Re = 300		Re = 500		Re = 800	
	CFD case	FSI case	CFD case	FSI case	CFD case	FSI case
0	0.342855	0.334139	0.221536	0.218223	0.157072	0.155413
2	0.347158	0.338239	0.222788	0.219411	0.156423	0.154701
4	0.360056	0.350603	0.228537	0.224991	0.15612	0.154361
6	0.38257	0.372627	0.239482	0.235677	0.16016	0.158443
8	0.414214	0.403517	0.256632	0.252632	0.168657	0.166945
10	0.451058	0.439229	0.278059	0.273645	0.180917	0.179107
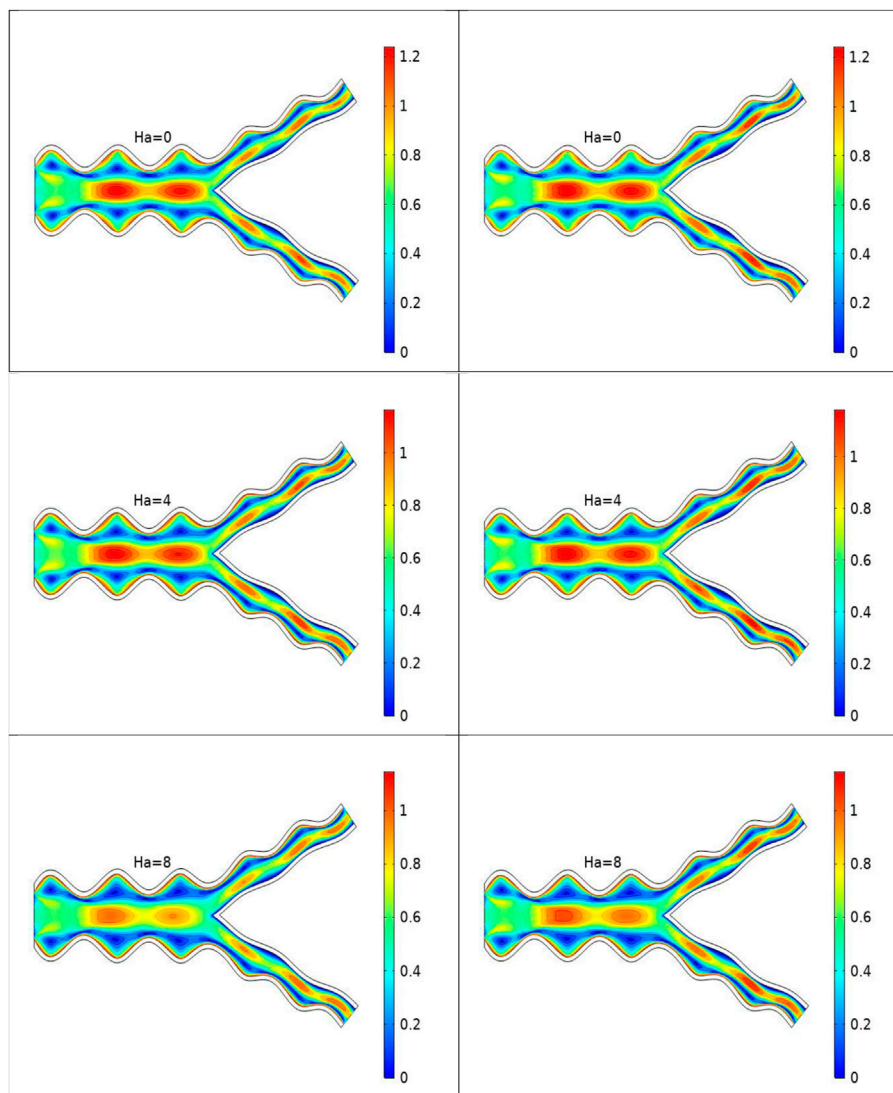
FIGURE 3
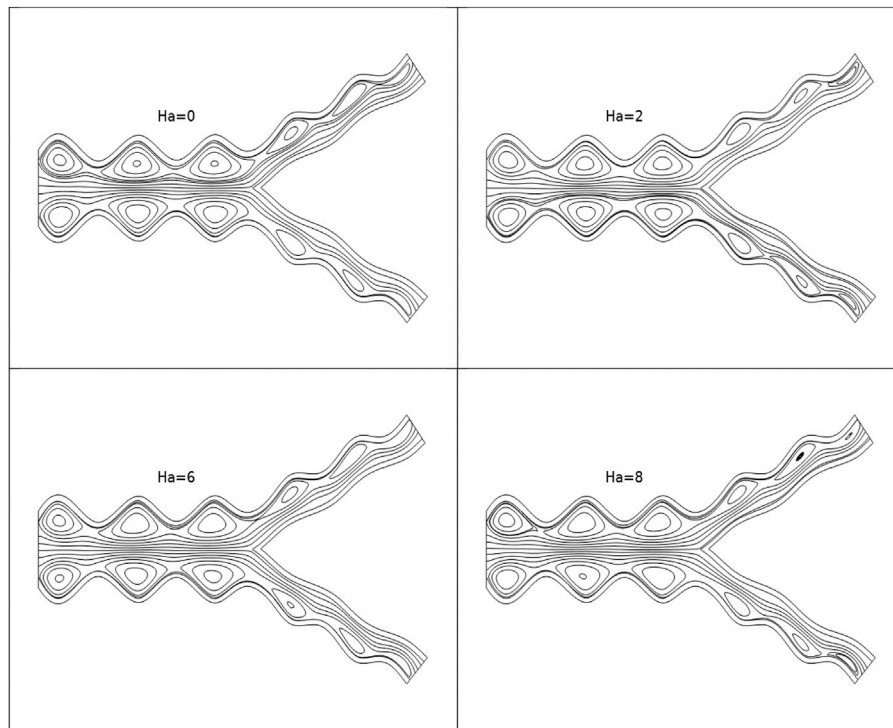Velocity contours for Re 300 (left) and 500 (right).

FIGURE 4
Streamlines for various Hartmann numbers at Re = 300.

Continuity equation

$$\frac{\partial u}{\partial x} + \frac{\partial v}{\partial y} = 0 \qquad (2)$$

Momentum equations

$$\rho\left((u - u_s)\frac{\partial u}{\partial x} + (v - v_s)\frac{\partial u}{\partial y} \right) = -\frac{\partial p}{\partial x} + \mu\left(\frac{\partial^2 u}{\partial x^2} + \frac{\partial^2 u}{\partial y^2} \right) - \sigma * B^2 * u$$

$$(3)$$

$$\rho\left((u - u_s)\frac{\partial v}{\partial x} + (v - v_s)\frac{\partial v}{\partial y} \right) = -\frac{\partial p}{\partial y} + \mu\left(\frac{\partial^2 v}{\partial x^2} + \frac{\partial^2 v}{\partial y^2} \right) \qquad (4)$$

The governing equation for the solid displacement is given by

$$\nabla \varrho_s = 0 \qquad (5)$$

where u, v, velocity component; u_s, v_s, mesh coordinate velocity; σ, electrical conductivity of the fluid; ρ, density of the fluid; μ, viscosity of the fluid; ϱ_s, solid stress tensor; B, magnetic field strength.

The elastic deformation of the walls caused by the fluid and pressure forces can be represented in terms of the Kirchhoff stress tensor as [36].

$$\tau = J\varrho_s$$
$$\varrho_s = J^{-1}FSF^T$$

where $F = (1 + \nabla d_s)$, $J = det(F)$, S is related by the strain ϵ as $S = C(E, \nu): (\epsilon)$, and

$$\epsilon = \frac{1}{2}\left(\nabla d_s + \nabla d_s^T + \nabla d_S^T \nabla d_s \right)$$

where S, second Piola-Kirchhoff stress tensor; E, Young's modulus; ν, Poisson's ratio; d_s, solid displacement vector.

Making use of the dimensionless variables listed bel

$$u = \frac{\bar{u}}{u_0}, \ v = \frac{\bar{v}}{u_0}, \ x = \frac{\bar{x}}{h}, \ y = \frac{\bar{y}}{h}, \ u_s = \frac{u_s}{u_0}, \ \varrho = \frac{\bar{\varrho}_s}{E}, \ p$$
$$= \frac{\bar{p}}{\rho u_0^2}, \ Re = \frac{\rho h u_0^2}{\mu}, \ Ha = \frac{\sigma B^2 h}{\mu} \qquad (6)$$

where h, channel height; u_0, inlet velocity; Re, Reynolds number; Ha, Hartmann number.

By taking a dimensionless parameter into account and omitting bar sign for simplicity, we can rewrite Eqs 2–5 as

$$\frac{\partial u}{\partial x} + \frac{\partial v}{\partial y} = 0 \qquad (7)$$

$$\rho\left((u - u_s)\frac{\partial u}{\partial x} + (v - v_s)\frac{\partial u}{\partial y} \right) = -\frac{\partial p}{\partial x} + \frac{1}{Re}\left(\frac{\partial^2 u}{\partial x^2} + \frac{\partial^2 u}{\partial y^2} \right)$$
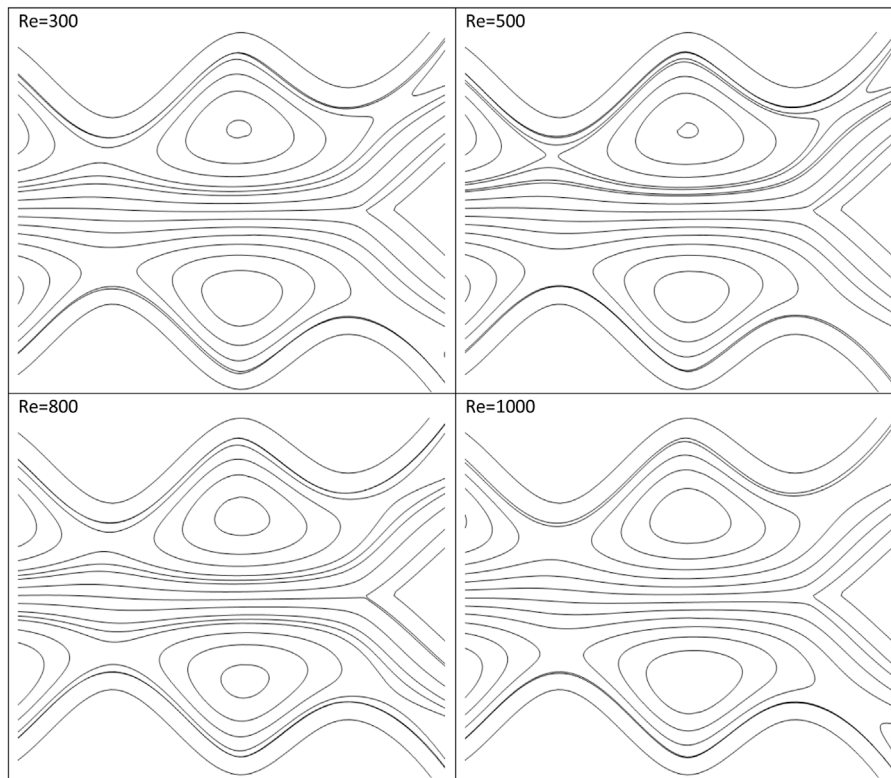$$- \frac{Ha^2}{Re} * u \qquad (8)$$

FIGURE 5
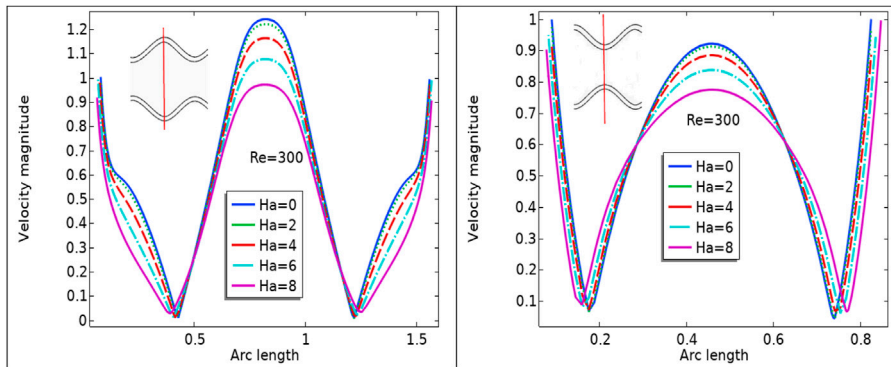Streamlines for various Reynolds numbers at Ha = 0.

FIGURE 6
Velocity profile for various cut lines defined.

$$\rho\left((u - u_s)\frac{\partial v}{\partial x} + (v - v_s)\frac{\partial v}{\partial y}\right) = -\frac{\partial p}{\partial y} + \frac{1}{Re}\left(\frac{\partial^2 v}{\partial x^2} + \frac{\partial^2 v}{\partial y^2}\right) \quad (9)$$

$$\nabla \varrho_s = 0 \quad (10)$$

At the inlet, a parabolic velocity profile is assumed as $u(x, y) = 3U_{max}\, y\,(1 - y)$. Pressure determines the outflow boundary conditions. The outlet's pressure is set to zero.

Solution methodology

To address the FSI problem, the interdependent system of partial differential Eqs 8–10 are solved with the ALE approach, based on FEM. Galerkin finite element method [35] was used to transform and discretize the equations. This approach combines the ability to move the boundary domain,
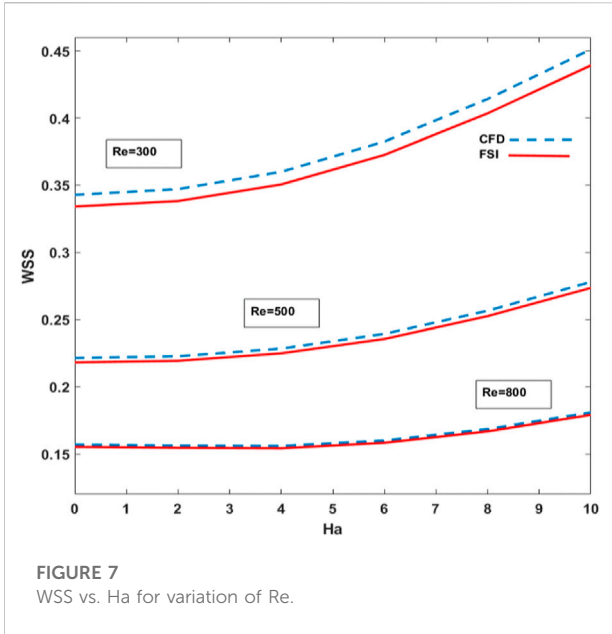
FIGURE 7
WSS vs. Ha for variation of Re.

holding a moving domain with a moving procedure. The ALE approach is explained in greater detail in the articles [37–41]. A solution accuracy is improved by applying hybrid mesh which consists of rectangular and triangular elements. The requirements for the nonlinear iteration's convergence are stated as

$$\left|\frac{\chi^{n-1} - \chi^n}{\chi^{n+1}}\right| < 10^{-6}$$

where χ is the general component of the solution. Figure 2 depicts the coarse level grid of the problem. The key steps to study the structural analysis of the domain using FEM are discretization, meshing, and mesh refinement. FEM schemes are used to address the complex fluid flow problems by dividing the domain into subdomains or elements. Since discretization of the domain into finite elements is a key step so meshing is performed at multiple levels but for optimization, only a coarse level is presented (see Figure 2). The first and second-order polynomial space (P_1 and P_2) is generated in the form of a hybrid grid consisting of quadrilateral and triangular elements to approximate the domain. Grid independence tests are performed to confirm that the results produced are independent of the number of mesh elements. The numerical values of WSS for the upper wall at Re = 200 and Ha = 0 are calculated for various refinement levels and shown in Table 1 (coarse to extremely fine). With the improvement of refinement
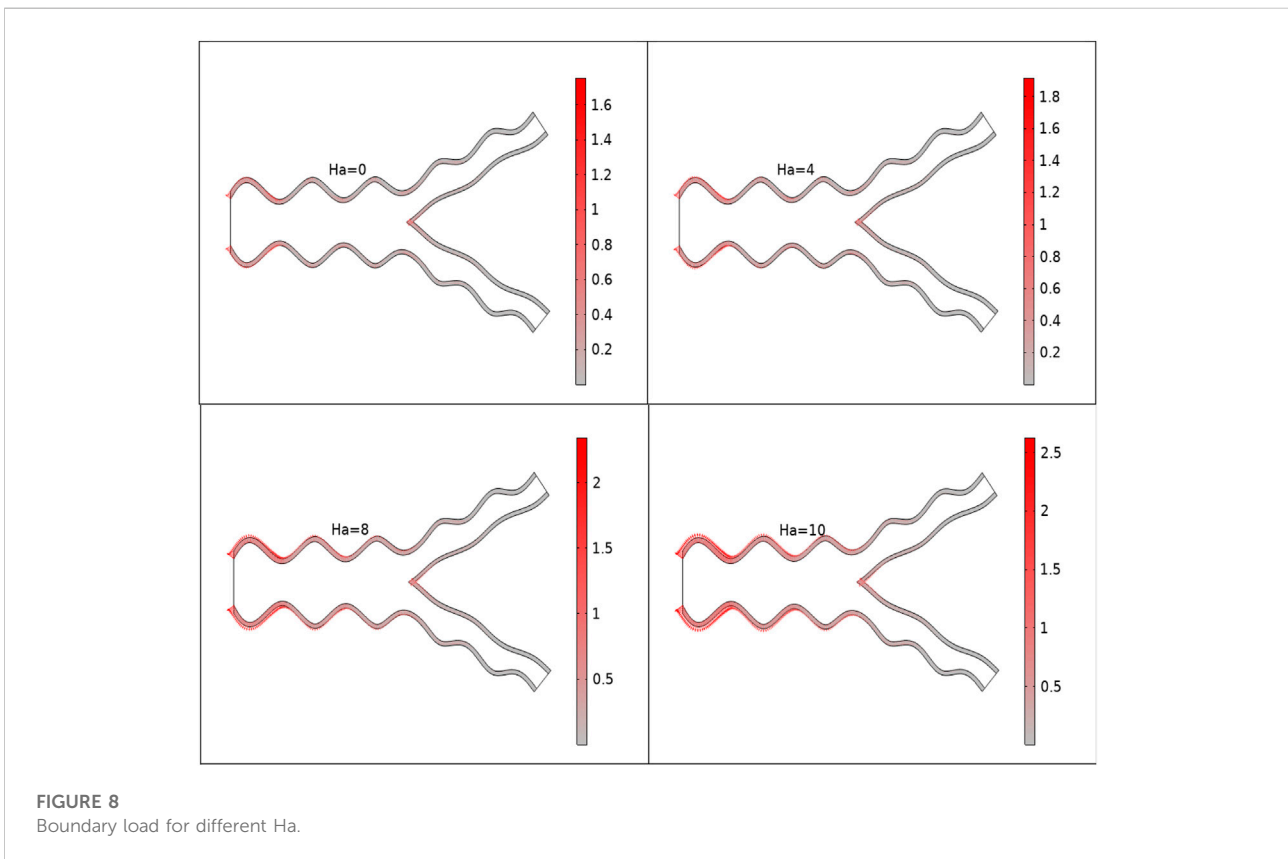

FIGURE 8
Boundary load for different Ha.

levels, the absolute error decreases and is minimum for extremely fine level. Therefore, the study is conducted at an extremely fine level.

Results and discussion

A two–dimensional theoretical model for bio-magnetic flow in a bifurcated channel with elastic wavy walls is proposed. The magnetic field is applied to the axial direction of the flow. The nonlinear differential equations are transformed into a dimensionless form by utilizing appropriate scales. The system of equations is discretized using ALE and is solved using the FEM approach. The numerical solution is obtained for the various values of the parameters involved. Results for various values of Ha and Re are produced to gain a physical understanding of the situation. The results are demonstrated by the mean of streamlines, velocity surfaces, displacements, and WSS.

In Table 2 WSS are calculated for the variation of Reynolds and Hartmann number. Also, a comparison is made for CFD (rigid wall) and FSI (elastic wall) cases. WSS decreases for the FSI case as compared to the CFD case where the walls of the channel are considered rigid. WSS decreases when the viscous forces inside the channel increase i. e for increasing Reynolds number. The magnetic field has opposite effects on WSS as compared to Re. WSS is minimum for pure hydrodynamic cases i.e., Ha = 0, but when the value of Hartmann number increases the pressure at the walls increases hence WSS increases (see Table 1).

Figure 3 shows the variation of velocity magnitude for various values of Hartmann number at Re = 300 (left) and 500 (right). Due to an increase in viscous forces the velocity magnitude inside the channel decreases. Therefore, an increase in Reynolds number retards the velocity. On the other hand velocity magnitude inside the channel is maximum for the pure hydrodynamic case. An increase in magnetic field strength give rise to WSS, as a result, velocity magnitude inside the channel decreases. Due to the elastic nature of the walls, a reasonable distortion can be observed for the variation of Hartmann number (see Figure 3). In Figure 4 streamlines are drawn for various values of the Hartmann number. Recirculation near the walls is maximum for the pure hydrodynamic case (Ha = 0). As Hartmann varies, the recirculation pattern decreases. The fluid exerts more pressure on the wall, which results in to increase in WSS. In Figure 5 streamlines for the variation of Reynolds number are drawn and observed near the bifurcation region. As increase in Reynolds number increases the viscous forces which consequently retards the flow and thereby reduced the flow velocity. This can also be observed by the recirculation pattern of the fluid near the

walls (see Figure 5). Figure 6 plots the velocity profile for the expanded and contracted region for the variation of Hartmann number. An increase in Hartmann's number reduces the velocity. Moreover, due to the parabolic inlet, a parabolic profile of velocity is observed.

Mechanical properties of the bifurcated channel are very important because they are directly related to recirculation area, flow pattern, WSS, etc. Due to the elastic behavior of wavy walls, a noticeable deformation can be seen for the variation of Hartmann number, which results in to decrease in the recirculation which gives rise to the wall shear stress. Figure 7 plots the WSS against the Hartmann number for the variation of Re. Also, a comparison is made between the CFD and FSI cases. A significant decrease in WSS for the FSI case. A boundary load is simulated in Figure 8. A significant change in the load at the boundary is observed for the variation of the Hartmann number. At Ha = 0, due to parabolic inlet velocity, there is a negligible load at the boundary. But it gradually starts increasing for variation of Ha. A noticeable change can be seen at Ha = 10.

Conclusion

A fluid-structure interaction study of two–dimensional biomagnetic flow in a bifurcated channel is conducted. The walls of the channel are assumed elastic. The magnetic field is applied to the axial direction of the flow. The nonlinear differential equations are transformed into a dimensionless form by utilizing appropriate scales. The system of equations is discretized using ALE and is solved using the FEM approach. The major findings of the study are highlighted as.

- WSS is higher for CFD (rigid wall) case as compared to FSI (elastic wall) case.
- WSS decreases for increasing values of Reynolds number.
- Compared to the pure hydrodynamic scenario, the magnetic field reduces the gain in velocity.
- There is an increase in the recirculation patterns near the walls of the channel for the variation of Hartmann number. Hence pressure exerted by the fluid on the wall increases.
- The magnetic field increases the boundary load as compared to the pure hydrodynamic case.
- The magnetic field increases the WSS and hence the risk of atherosclerosis reduces.

Data availability statement

The raw data supporting the conclusion of this article will be made available by the authors, without undue reservation.

Author contributions

ZR: funding; HS and AHM computed the results; HS and SME wrote the original draft; XW has supervised; AR and AHM wrote the review draft; XW and MAA: modeling; Conceptualization and Validation, MAA.

Funding

Conflict of interest

The authors declare that the research was conducted in the absence of any commercial or financial relationships that could be construed as a potential conflict of interest.

Publisher's note

All claims expressed in this article are solely those of the authors and do not necessarily represent those of their affiliated organizations, or those of the publisher, the editors and the reviewers. Any product that may be evaluated in this article, or claim that may be made by its manufacturer, is not guaranteed or endorsed by the publisher.

References

1. Lloyd-Jones D, Adams RJ, Brown TM, Carnethon M, Dai S, De Simone G, et al. Heart disease and stroke statistics-2010 update: A report from the American heart Association. *Circulation* (2010) 121:e46–e215. doi:10.1161/CIRCULATIONAHA.109.192667

2. Jackson SP. Arterial thrombosis-insidious, unpredictable and deadly. *Nat Med* (2011) 17:1423–36. doi:10.1038/nm.2515

3. Davies MJ, Fulton WF, Robertson WB. The relation of coronary thrombosis to ischaemic myocardial necrosis. *J. Pathol.* (1979) 127:99–110. doi:10.1002/path.1711270208

4. Srinivasacharya D, Madhava Rao G. Modeling of blood flow through a bifurcated artery using nanofluid. *Bionanoscience* (2017) 7:464–74. doi:10.1007/s12668-017-0402-6

5. Ahmed A. Peristaltic flow of a magnetohydrodynamic nanofluid through a bifurcated channel. *Acta Mech* (2021) 232:575–89. doi:10.1007/s00707-020-02731-6

6. Fojas JJR, De Leon RL. Carotid artery modeling using the Navier-Stokes equations for an incompressible, Newtonian and Axisymmetric flow. *APCBEE Proced* (2013) 7:86–92. doi:10.1016/j.apcbee.2013.08.017

7. Chang HK, El Masry OA. A model study of flow dynamics in human central airways. Part I: Axial velocity profiles. *Respir Physiol* (1982) 49:75–95. doi:10.1016/0034-5687(82)90104-9

8. Schroter RC, Sudlow MF. Flow patterns in models of the human bronchial airways. *Respir Physiol* (1969) 7:341–55. doi:10.1016/0034-5687(69)90018-8

9. Pedley TJ, Schroter RC, Sudlow MF. Energy losses and pressure drop in models of human airways. *Respir Physiol* (1970) 9:371–86. doi:10.1016/0034-5687(70)90093-9

10. Pedley TJ, Schroter RC, Sudlow MF. The prediction of pressure drop and variation of resistance within the human bronchial airways. *Respir Physiol* (1970) 9:387–405. doi:10.1016/0034-5687(70)90094-0

11. Mekheimer KS, Abo-Elkhair RE, Abdelsalam SI, Ali KK, Moawad AMA. Biomedical simulations of nanoparticles drug delivery to blood hemodynamics in diseased organs: Synovitis problem. *Int Commun Heat Mass Transfer* (2021) 130:105756. doi:10.1016/j.icheatmasstransfer.2021.105756

12. Smith FT. On entry-flow effects in bifurcating, blocked or constricted tubes. *J Fluid Mech* (1976) 78:709–36. doi:10.1017/S002211207600270X

13. Yung CN, de Witt KJ, Keith TG. Three-dimensional steady flow through a bifurcation. *J Biomech Eng* (1990) 112:189–97. doi:10.1115/1.2891171

14. Zhao Y, Lieber BB. Steady Inspiratory flow in a model Symmetric bifurcation. *J Biomech Eng* (2016) 116:488–96. doi:10.1115/1.2895800

15. Zhao Y, Lieber BB. Steady expiratory flow in a model Symmetric bifurcation. *J Biomech Eng* (2016) 116:318–23. doi:10.1115/1.2895737

16. Zhao Y, Brunskill CT, Lieber BB. Inspiratory and expiratory steady flow analysis in a model symmetrically bifurcating airway. *J Biomech Eng* (1997) 119:52–8. doi:10.1115/1.2796064

17. Kolin A. An electromagnetic flowmeter: The principle of the method and its application to blood flow measurements. *Exp Biol Med (Maywood)* (1936) 35:53–6. doi:10.3181/00379727-35-8854p

18. Korchevskii LS, Marochnik EM. Magnetohydrodynamic version of movement of blood. *Biophys* (1965) 10:411–3. doi:10.1016/j.asej.2016.04.023

19. Ahmed Z, Nadeem S, Saleem S, Ellahi R. Numerical study of unsteady flow and heat transfer CNT-based MHD nanofluid with variable viscosity over a permeable shrinking surface. *Int J Numer Methods Heat Fluid Flow* (2019) 29:4607–23. doi:10.1108/HFF-04-2019-0346

20. Srinivasacharya D, Rao M. Computational analysis of magnetic effects on pulsatile flow of couple stress fluid through a bifurcated artery. *Comput Methods Programs Biomed* (2016) 137:269–79. doi:10.1016/j.cmpb.2016.09.015

21. Abdelsalam SI, Mekheimer KS, Zaher AZ. Dynamism of a hybrid Casson nanofluid with laser radiation and chemical reaction through sinusoidal channels. *Waves in Random and Complex Media* (2022). 2022. 1–22. doi:10.1080/17455030.2022.2058714

22. Jagadeesha RD, Prasanna BMR, Sankar M. Double diffusive convection in an inclined parallelogrammic porous enclosure. *Proced Eng* (2015) 127:1346–53. doi:10.1016/j.proeng.2015.11.493

23. Jagadeesha RD, Prasanna BMR, Younghae D, Sankar M. Natural convection in an inclined parallelogrammic porous enclosure under the effect of magnetic field. *J Phys : Conf Ser* (2017) 908:012076. doi:10.1088/1742-6596/908/1/012076

24. Alsharif AM, Abdellateef AI, Elmaboud YA, Abdelsalam SI. Performance enhancement of a DC-operated micropump with electroosmosis in a hybrid nanofluid: Fractional Cattaneo heat flux problem. *Appl Math Mech* (2022) 43(6):931–44. doi:10.1007/s10483-022-2854-6

25. Shahzad H, Ain QU, Pasha AA, Irshad K, Shah IA, Ghaffari A, et al. Double-diffusive natural convection energy transfer in magnetically influenced Casson fluid flow in trapezoidal enclosure with fillets. *Int Commun Heat Mass Transfer* (2022) 137:106236. doi:10.1016/j.icheatmasstransfer.2022.106236

26. Crosetto P, Reymond P, Deparis S, Kontaxakis D, Stergiopulos N, Quarteroni A. Fluid-structure interaction simulation of aortic blood flow. *Comput Fluids* (2011) 43:46–57. doi:10.1016/j.compfluid.2010.11.032

27. Idelsohn SR, Oñate E, Del Pin F. A Lagrangian meshless finite element method applied to fluid-structure interaction problems. *Comput Struct* (2003) 81:655–71. doi:10.1016/S0045-7949(02)00477-7

28. Cottet GH, Maitre E, Milcent T. Eulerian formulation and level set models for incompressible. *Fluid-Structure Interaction* (2008) 42:471–92. doi:10.1051/m2an

29. Scovazzi G, Hughes TJR. Lecture Notes on continuum mechanics on arbitrary moving domains. *Solutions* (2007) 62.

30. Zhao YC, Vatankhah P, Goh T, Wang J, Chen XV, Kashani MN, et al. Computational fluid dynamics simulations at micro-scale stenosis for microfluidic thrombosis model characterization. *Mol Cel Biomech* (2021) 18:1–10. doi:10.32604/mcb.2021.012598

31. Methods C, Mech A, Bazilevs Y, Gohean JR, Hughes TJR, Moser RD, et al. Patient-specific isogeometric fluid-structure interaction analysis of thoracic aortic blood flow due to implantation of the Jarvik 2000 left ventricular assist device. *Comput Methods Appl Mech Eng* (2009) 198:3534–50. doi:10.1016/j.cma.2009. 04.015

32. Nobile F. *Numerical approximation of fluid-structure interaction problems with applications to Haemodynamics*. Lausanne: EPFL (2001). doi:10.5075/epfl-thesis-2458

33. Shahzad H, Wang X, Sarris I, Iqbal K, Hafeez MB, Krawczuk M. Study of Non - Newtonian biomagnetic blood flow in a stenosed bifurcated artery having elastic walls. *Sci Rep* (2021) 11:23835. doi:10.1038/s41598-021-03426-1

34. Anwar MA, Iqbal K, Razzaq M. Analysis of biomagnetic blood flow in a stenosed bifurcation artery amidst elastic walls. *Phys Scr* (2021) 96:085202. doi:10. 1088/1402-4896/abf67b

35. Sajid M, Shahzad H, Mughees M, Ali N. Mathematical modeling of slip and magnetohydrodynamics effects in blade coating. *J Plast Film Sheeting* (2019) 35: 9–21. doi:10.1177/8756087918777782

36. Ghalambaz M, Jamesahar E, Ismael MA, Chamkha AJ. Fluid-structure interaction study of natural convection heat transfer over a flexible oscillating fin in a square cavity. *Int J Therm Sci* (2017) 111:256–73. doi:10.1016/j.ijthermalsci. 2016.09.001

37. Casadei F, Halleux JP. An algorithm for permanent fluid-structure interaction in explicit transient dynamics. *Comput Methods Appl Mech Eng* (1995) 128:231–89. doi:10.1016/0045-7825(95)00843-8

38. Donea J, Huerta A. *Finite element methods for flow problems*. Hoboken: Wiley (2003). p. 30.

39. Donea J, Giuliani S, Halleux JP. An arbitrary Lagrangian-Eulerian finite element method for transient dynamic fluid-structure interactions. *Comput Methods Appl Mech Eng* (1982) 33:689–723. doi:10.1016/0045-7825(82) 90128-1

40. Kuhl E, Hulshof S, de Borst R. An arbitrary Lagrangian eulerian finite-element approach for fluid-structure interaction phenomena. *Int J Numer Methods Eng* (2003) 57:117–42. doi:10.1002/nme.749

41. Mazumder S. *Numerical methods for partial differential equations: Finite difference and finite volume methods*. Cambridge: Academic Press (2015).